


ARTICLE



<https://doi.org/10.1038/s41467-022-30726-5>

OPEN

Optical linewidth of soliton microcombs

Fuchuan Lei ¹, Zhichao Ye¹, Óskar B. Helgason¹, Attila Fülöp¹, Marcello Girardi¹ & Victor Torres-Company ¹✉

Soliton microcombs provide a versatile platform for realizing fundamental studies and technological applications. To be utilized as frequency rulers for precision metrology, soliton microcombs must display broadband phase coherence, a parameter characterized by the optical phase or frequency noise of the comb lines and their corresponding optical linewidths. Here, we analyse the optical phase-noise dynamics in soliton microcombs generated in silicon nitride high-Q microresonators and show that, because of the Raman self-frequency shift or dispersive-wave recoil, the Lorentzian linewidth of some of the comb lines can, surprisingly, be narrower than that of the pump laser. This work elucidates information about the physical limits in phase coherence of soliton microcombs and illustrates a new strategy for the generation of spectrally coherent light on chip.

¹Department of Microtechnology and Nanoscience, Chalmers University of Technology, SE-41296 Gothenburg, Sweden. ✉email: torresv@chalmers.se

The study of the laser's linewidth started with the seminal works of Schawlow and Townes¹, even before the invention of the laser. For an ideal laser oscillator, the frequency noise power spectral density (PSD) is a constant that determines the oscillator linewidth². In practice, the PSD of a laser is far richer and complex³. The laser linewidth derived from the flat region at high offset frequencies in the PSD is called intrinsic (or Lorentzian) as it arises from white frequency noise which cannot be effectively suppressed through a finite-bandwidth feedback control loop. The Lorentzian linewidth hence represents the ultimate performance in temporal coherence of an oscillator. Recent breakthroughs in silicon photonics have demonstrated integrated laser oscillators with a Lorentzian linewidth at the Hz (and below) level^{4,5}. In optical coherent communications, the Lorentzian linewidth is a key metric, as it determines the instantaneous frequency and phase fluctuations on a short time scale that must be tracked with sufficient accuracy by the receiver for efficient distortion compensation⁶.

A frequency comb is a laser whose spectrum is composed of equidistant frequency components that are phase locked to a common frequency reference. The phase noise of the constituent optical lines sets a physical limit on the achievable time and frequency stability^{7–9}. Significant efforts have been devoted to the systematic understanding of the linewidth of mode-locked lasers and frequency combs based on solid-state^{10,11}, semiconductor¹², and fiber lasers^{13,14}. In 2007, a new type of frequency comb source (microcomb) was demonstrated¹⁵. Microcombs harness the Kerr nonlinearity and large intensity buildup in a high-Q microresonator cavity. Low-noise coherent states can be attained through the generation of dissipative solitons^{16–18}. Unlike in conventional frequency combs based on mode-locked lasers, where the gain originates from stimulated emission in active gain media and the Lorentzian linewidth is partially dictated by spontaneous emission, the gain of soliton microcombs is based on resonantly enhanced continuous-wave-pumped parametric amplification, and the noise caused by spontaneous scattering is very weak. Another important difference is that in microcombs, the pump laser is coherently added to the comb spectrum, and therefore its noise is expected to be transferred equally to all comb lines. Indeed, earlier studies demonstrated that when the microcomb operates in a low-noise state, the comb lines inherit the linewidth of the pump^{19,20}, with lines further away degrading more due to thermo-refractive noise (TRN) in the cavity^{21,22}.

In this work, we present both theoretical and experimental studies of the Lorentzian linewidth of soliton microcombs. We reveal that the interplay between the pump's frequency noise and soliton dynamics results in a linewidth distribution among comb lines that is consistent with the elastic-tape model²³, akin to what has been found previously with conventional mode-locked frequency combs^{11,12,14}. An important difference in soliton microcombs is that the Raman self-frequency shift and dispersive-wave recoil couple the repetition rate of the soliton with the pump frequency^{24,25}. This results in a subset of comb lines becoming resilient to the frequency noise of the pump laser, and an encompassing decrease in Lorentzian linewidth. Our work provides a comprehensive understanding of the optical phase noise dynamics in soliton microcombs. Furthermore, the mechanism for the reduction of the pump linewidth provides a new strategy to generate ultra-low-phase-noise coherent optical oscillators on chip.

Results

Elastic-tape model applied to soliton microcombs. In this section, we analyse from a theoretical perspective the Lorentzian linewidth of soliton microcombs. Concretely, we analyze the flat frequency noise component of the PSD of the different comb

lines. In general, both the pump laser's phase noise and intensity noise have an impact on the Lorentzian linewidth of the comb lines. In addition, we shall consider shot noise affecting both the pump laser and the cavity, as an additive zero-point fluctuation field²⁶ (see Fig. 1a). TRN leaves its footprint in the low-offset frequency region of the PSD²⁷. As a result, it will influence the effective linewidth, an aspect that will be addressed in the latter sections.

We begin by considering the contribution of the frequency noise of the pump. The optical frequency of the m -th microcomb line ν_m is determined by two degrees of freedom, i.e., the frequency of the pump laser ν_p and the repetition rate of the soliton microcomb ν_{rep} ,

$$\nu_m = \nu_p + m\nu_{\text{rep}}, \quad (1)$$

with the comb line number, m , counted from the pump. The underlying assumption in the elastic-tape model²³ is that the noise sources will result in collective fluctuations of the comb lines. According to this, equation (1) indicates that the linewidth of the pump would be faithfully imprinted on all other comb lines if the repetition rate were fixed. However, in soliton microcombs, due to the existence of intrinsic intrapulse Raman scattering²⁴ and dispersive-wave recoil^{28–30}, the pump phase noise will also affect the repetition rate. The repetition rate can be written as²⁵

$$\nu_{\text{rep}} = \frac{1}{2\pi} \left[D_1 + \frac{D_2}{D_1} (\Omega_{\text{Raman}} + \Omega_{\text{Recoil}}) \right], \quad (2)$$

where $D_1/2\pi$ is the cavity's free spectral range (FSR) at the pump mode, and $D_2 = -D_1^2\beta_2/\beta_1$ with β_1 and β_2 being the first- and second-order coefficients of the Taylor expansion of the mode propagation constant β^3 . Ω_{Raman} and Ω_{Recoil} denote the shift of the carrier frequency due to Raman scattering, i.e., the Raman self-frequency shift²⁴ and dispersive-wave recoil²⁵, and both are functions of the detuning between the pump's cavity mode and the laser frequency, $(\nu_c - \nu_p)$ ^{25,32}. For simplicity, we only consider the Raman term in the main text, while the effect of dispersive-wave recoil is discussed in Supplementary Note 1.

According to Eqs. (1) and (2), the frequency change of the m -th comb line $\delta\nu_m$ induced by that of the pump $\delta\nu_p$ can be written as

$$\delta\nu_m = \delta\nu_p \left(1 + m \frac{d\nu_{\text{rep}}}{d\nu_p} \right). \quad (3)$$

In the following, we will characterize the frequency noise of the comb lines by means of the frequency noise PSD, $S_{\Delta\nu,m}(f)$, (sometimes called FM noise). When flicker noise and other technical sources are neglected, the pump frequency noise PSD $S_{\Delta\nu}^p(f)$ is characterized by a constant level and has a simple relation with its fundamental phase noise PSD $S_{\Delta\phi}^p$ as

$$S_{\Delta\nu}^p(f) = f^2 S_{\Delta\phi}^p(f) = S_0. \quad (4)$$

The full-width at half maximum accounts for the Lorentzian linewidth, $\Delta\nu_p = \pi S_0$ ^{11,33}. From equation (3), the frequency noise PSD of the m -th comb line, $S_{\Delta\nu,m}(f)$, can be directly linked to the frequency noise PSD of the pump as

$$S_{\Delta\nu,m}(f) = S_{\Delta\nu}^p(f) \left(1 - \frac{m}{m_{\text{fix}}} \right)^2. \quad (5)$$

where $m_{\text{fix}} = -(d\nu_{\text{rep}}/d\nu_p)^{-1}$ corresponds to the pump phase-noise fixed point²³. Equation (5) indicates that the Lorentzian linewidth of the microcomb induced by the pump linewidth follows a parabolic distribution with line number, with a minimum value reaching zero at the fixed point, see Fig. 1. For soliton microcombs affected by the Raman self-frequency shift,

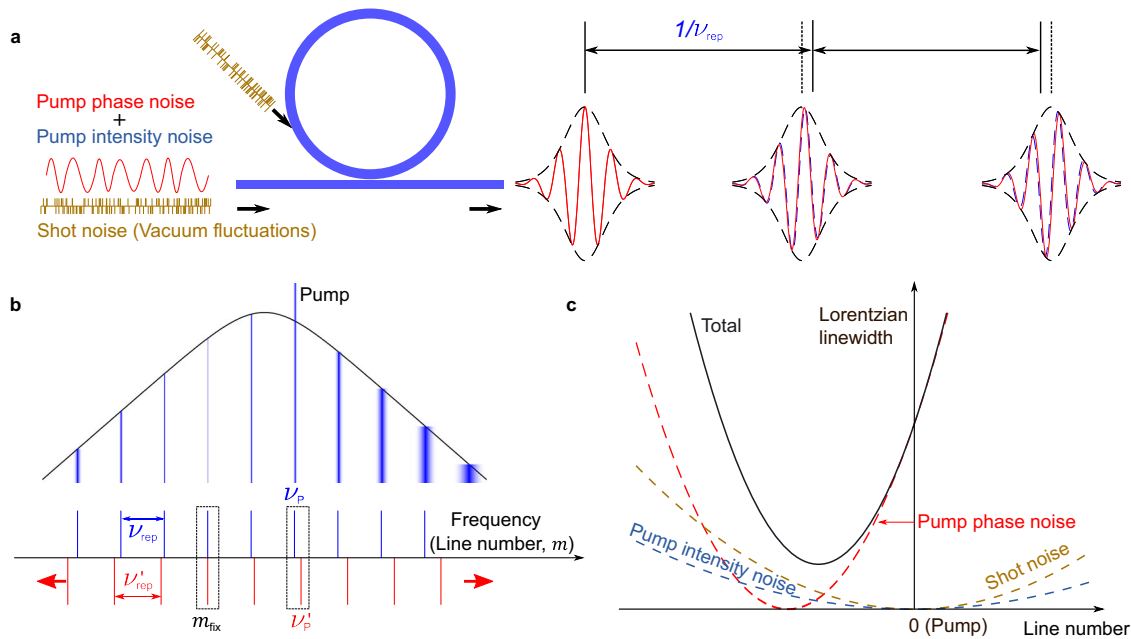


Fig. 1 Noise-induced frequency fluctuations and optical linewidth narrowing in soliton microcombs. **a** Soliton microcombs are generated by coupling a continuous-wave laser into a longitudinal mode of a high-Q microresonator. The phase and intensity noise of the pump and shot noise (vacuum fluctuations) cause timing jitter and pulse carrier-envelope offset fluctuations that result into a finite optical linewidth of the frequency comb lines. **b** Because of the Raman self-frequency shift, variations in pump’s laser frequency to the blue side result in an increase of the soliton repetition rate, and vice versa to the red side. The coupling between pump frequency and repetition rate thus results in the existence of a so-called “fixed point” in the comb spectrum, that is a comb line that is most resilient to the fluctuations of the pump’s frequency noise. This translates into a Lorentzian linewidth distribution with line number whose minimum can be located far away from the pump. **c** The shot noise and pump intensity noise affect directly the timing jitter of the soliton pulse train, which results in a linewidth distribution symmetrically located around the pump. These three effects together set the lowest achievable Lorentzian linewidth of soliton microcombs.

the fixed point appears on the red side of the pump because the repetition rate increases when the pump frequency increases. While the dispersive-wave recoil induced by third-order dispersion or mode coupling can modify the location of the fixed point (Supplementary Note 1). Importantly, the elastic-tape model applies in these two cases, in spite of different physical mechanisms coupling the repetition rate with detuning.

In addition to the pump phase noise, the shot noise can also introduce frequency noise into the soliton microcomb. In the studies of supercontinuum generation, shot noise poses fundamental limitations in the achievable spectral coherence^{34,35}. In soliton microcombs, the shot noise hardly affects the pump frequency, however, it sets a fundamental-limited timing jitter^{26,36–38}. As the repetition rate is mainly determined by D_1 , the timing jitter PSD, $S_{tm}^Q(f)$, affects the optical frequency noise of the comb lines $S_{\Delta\nu,m}(f)$ through

$$S_{\Delta\nu,m}(f) = m^2 f^2 D_1^2 S_{tm}^Q(f). \tag{6}$$

With the fact $S_{tm}^Q(f) \propto 1/f^2$ if $f \ll \nu_p/Q$ ^{26,36}, one can see that the shot noise leads to a line-number-dependent white optical frequency noise. Since the effect arising from spontaneous Raman scattering is usually much weaker than the shot noise³⁴, it is ignored here.

In addition to the above two fundamental noise sources with quantum origin, in practice the intensity noise of the pump could also introduce frequency noise into the soliton microcomb because the repetition rate can be modified by the pump power via the Raman and dispersive-wave emission, but with little influence on the pump frequency. The frequency noise PSD induced by the relative intensity noise (RIN) of the pump $S_{RIN}^p(f)$

can be written as

$$S_{\Delta\nu,m}(f) = m^2 f^2 D_1^2 S_{tm}^{RIN}(f). \tag{7}$$

where the RIN-noise-induced timing jitter $S_{tm}^{RIN}(f) \propto S_{RIN}^p(f)/f^2$ if $f \ll \nu_p/Q$. Note that the frequency dependence of the $S_{RIN}^p(f)$ may be dominated by flicker noise. However, only its white frequency component is accounted for in the Lorentzian linewidth. As illustrated in Fig. 1c, the intensity noise introduces a parabolic distribution of the Lorentzian linewidth whose center is located at the pump mode.

Since the above three noise sources (pump’s intensity and phase noise, and shot noise) are independent of each other, their individual contribution to the linewidth can be added together. Thus, the Lorentzian linewidth of the m -th line of a single-soliton microcomb can be expressed as

$$\Delta\nu_m = \Delta\nu_p \left(1 - \frac{m}{m_{fix}}\right)^2 + m^2(\Delta\nu_{RIN} + \Delta\nu_Q) \tag{8}$$

with $\Delta\nu_{RIN} = \pi D_1^2 f^2 S_{tm}^{RIN}(f)$ and $\Delta\nu_Q = \pi D_1^2 f^2 S_{tm}^Q(f)$. Equation (8) illustrates that because of the timing jitter induced by shot noise and intensity noise, the comb line with the minimum Lorentzian linewidth (we term it here the *quiet mode*) is no longer the phase-noise fixed point, and its location appears closer to the pump but remains always to the longer-wavelength side (see Fig. 1c). It is instructive to manipulate further equation (8) and calculate the reduction of the linewidth at the quiet mode, $\Delta\nu_{min}$, relative to the pump’s Lorentzian linewidth

$$\frac{\Delta\nu_p}{\Delta\nu_{min}} = 1 + \frac{1}{m_{fix}^2} \frac{\Delta\nu_p}{\Delta\nu_Q + \Delta\nu_{RIN}}. \tag{9}$$

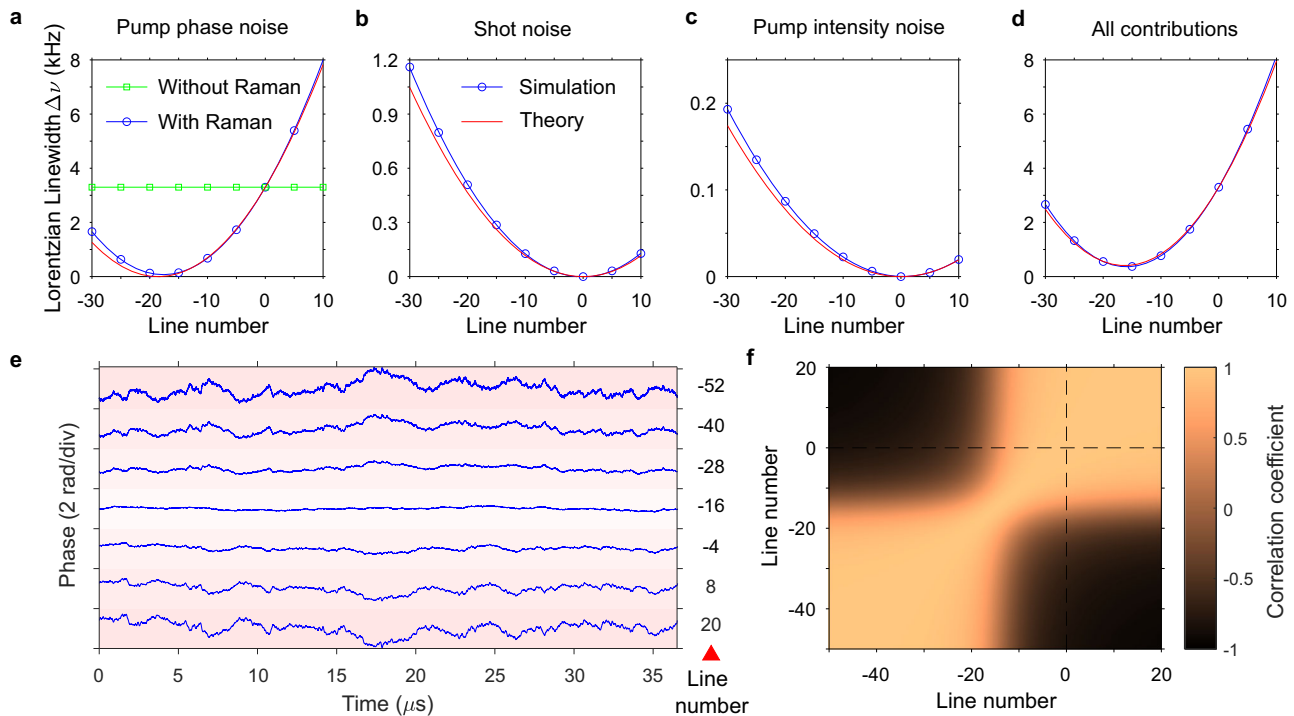


Fig. 2 Numerical study of the Lorentzian linewidth of soliton microcombs. The Lorentzian linewidth of comb lines induced by pump phase noise, shot noise, pump intensity noise and when all noise sources are included, from **a** to **d**. The squares and circles denote the simulated data. The theoretical results in **a–d** (red lines) are calculated according to Eqs. (5)–(8). **e** Phase fluctuations of selected comb lines. **f** Phase correlation among comb lines, computed according to Eq. (10).

Equation (9) indicates that the relative reduction in linewidth is more prominent for pump lasers with larger Lorentzian linewidths. This observation allows for decreasing the Lorentzian linewidth of a coherent oscillator by performing frequency translation to the quiet mode with the aid of a soliton microcomb, an aspect that is addressed experimentally in the Supplementary Note 2.

Optical phase noise dynamics and numerical simulations. To test the validity of the previous theoretical analysis and gain a better understanding, we conduct a series of numerical simulations based on the Ikeda map^{39,40}. The parameters of the simulations are chosen to match the characteristics of our silicon nitride (SiN) microresonators and are detailed in the “Methods” section. The simulations also allow us to study the influence of the individual contribution of the different noise sources on the dynamics of the Lorentzian linewidth of soliton microcombs. We begin the analysis by considering the optical phase noise of the pump only (Fig. 2a). In absence of Raman self-frequency shift, for a coherent dissipative soliton state, the phase noise is transduced equally among the comb lines, indicating a tight phase locking with the pump. However, when the Raman term is included, fluctuations in pump frequency are transduced into repetition rate changes. The repetition rate increases with detuning as a result of the Raman self-frequency shift, resulting in a fixed point on the red side of the pump characterized by near-zero frequency fluctuations in theory and validated by the simulations.

As anticipated in the previous section, both shot noise and intensity noise prevent us from attaining a near zero Lorentzian linewidth at the fixed point. This is analyzed in the numerical simulations presented in Fig. 2b, c. Since shot noise and intensity noise do not modify the frequency of the pump but the repetition rate of the soliton microcomb, the distribution of the linewidth is

symmetric with respect to the pump and follows a parabolic profile, in agreement with the theoretical analysis presented in the previous section, cf. Eqs. (6) and (7). Note that the Lorentzian linewidth induced by shot-noise timing jitter in our SiN microcomb is more than one order of magnitude higher than what has been previously reported for silica microcombs³⁶, mainly due to the larger nonlinear coefficient of the SiN cavity mode. Hence, the shot noise sets a relatively high bound to the lowest achievable Lorentzian linewidth in this platform. Figure 2d shows the simulation results when all noise contributions are added together. The Lorentzian linewidth based on the theoretical model (Eq. (8)) is plotted for comparison. The agreement between the theory and simulation indicates the elastic tape models can account for the most salient features of the optical phase noise dynamics in soliton microcombs. The slight deviation may arise from the fact that the elastic tape model implicitly assumes an instantaneous response in the two degrees of freedom of the comb, whereas in reality, there is an intrinsic latency in the system that can cause the comb to fluctuate in more than two degrees of freedom.

We end this section by analyzing the phase noise dynamics of the individual line components when all noise sources are included. Specifically, we compute the phase noise of individual frequency lines, see Fig. 2e. Clearly, the lines close to the quiet mode display reduced phase noise, with a standard deviation smaller than the inherent phase noise of the pump laser. Remarkably, the quiet mode stands out as a mirror symmetry point in the comb, whereby lines symmetrically located around it attain identical Lorentzian linewidth but anti-correlated phase noise. A similar behavior has been observed before for electro-optic frequency combs, with the key difference that the fixed point corresponds there to the pump laser frequency^{41,42}. This observation can be further quantified with the aid of the Pearson’s

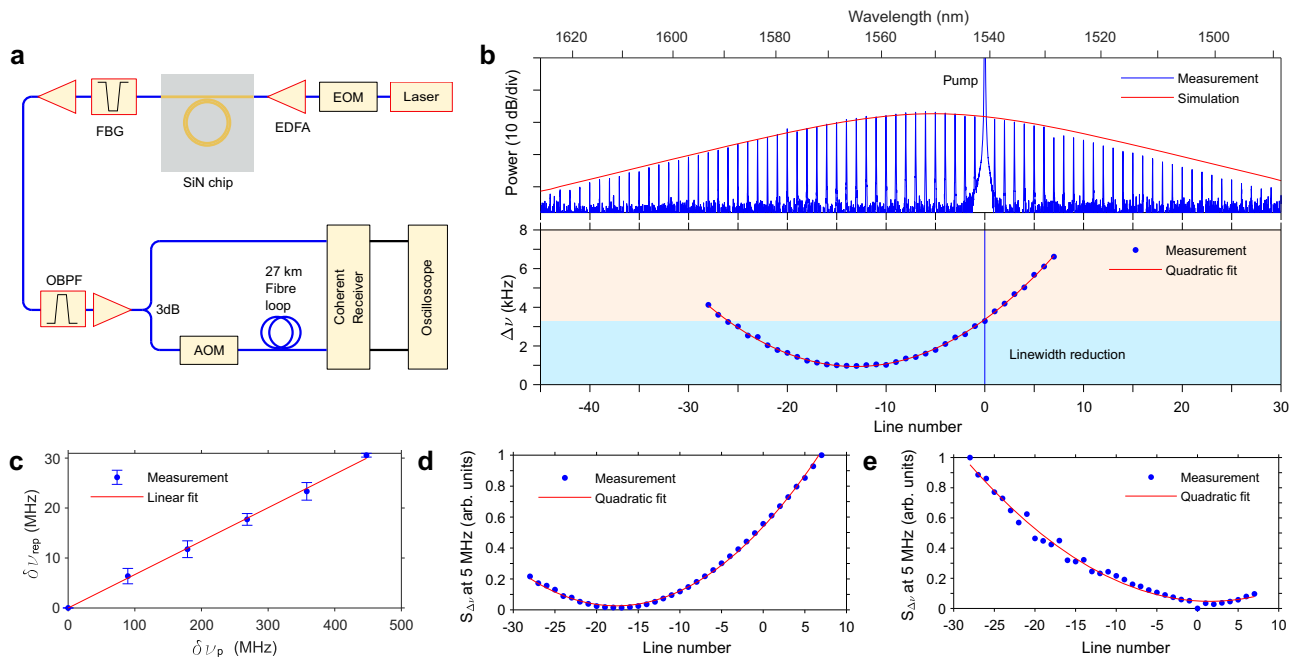


Fig. 3 Experimental study of the Lorentzian linewidth of silicon nitride soliton microcombs. **a** Setup for linewidth measurement. EOM, (Phase or Intensity) Electro-optical modulator; EDFA, Erbium-doped fiber amplifier; FBG, Fiber Bragg grating for pump rejection; OBPF, Optical band-pass filter; AOM, Acousto-optic modulator. **b** The optical spectrum of the single-soliton microcomb and the measured Lorentzian linewidth of comb lines according to the mean value of $S_{\Delta\nu,m}(f)$ at high offset frequencies ranging from 3 to 5 MHz. **c** Measured dependence of soliton microcomb repetition rate change in terms of relative pump frequency. The error bar stands for the standard deviation of three measurements. **d, e** The height of frequency noise PSD at 5 MHz, originating from applying a phase or intensity modulation signal to the pump, respectively.

correlation coefficient:

$$C(m, n) = \frac{\text{cov}(\phi_m, \phi_n)}{\sigma_{\phi_m} \sigma_{\phi_n}}, \quad (10)$$

where ϕ_m denotes the sampled phase for the m -th comb line. cov is the covariance and σ_X is the standard deviation of X . The result is plotted in Fig. 2f. One can see that the phases of comb lines at the same side of $m = -16$ are highly correlated, and those on opposite sides anti-correlated, which can be explained with the elastic-tape model¹¹.

Experiments with SiN microcombs. We present experimental results of the distribution of the frequency noise and corresponding Lorentzian linewidth in a soliton microcomb implemented in a silicon nitride microresonator pumped by a narrow-linewidth external-cavity tunable diode laser (Santec TLS 710). The setup is shown in Fig. 3a. The FSR and the average intrinsic Q factor of the SiN microresonator are 227.5 GHz and 1.16×10^7 . The pump laser is amplified by an EDFA. The power coupled into the bus waveguide is 120 mW. Other parameters and experimental details are described in the Methods. The soliton microcomb generation is enabled through fast thermo-optic tuning via an integrated metallic heater⁴³. The optical spectrum of the generated single-soliton microcomb is shown in Fig. 3b. After attenuation of the pump line with a notch filter, the comb is amplified with either a C- or L-band EDFA. Then each comb line is filtered out separately and amplified to ~20 mW. Subsequently, the phase and frequency noise of each comb line is measured through a self-heterodyne measurement technique implemented with the aid of a coherent receiver (Neophotonics, 100 Gbps micro-ICR)³³.

The measured Lorentzian linewidth for the comb lines from $m = -28$ to $m = 7$ is shown in Fig. 3b, which is obtained based on the average value at high offset frequencies (3–5 MHz) of the

frequency noise PSD (Supplementary Note 3)⁴. This region is chosen to avoid the contribution of flicker noise at low frequencies and the divergence at high frequencies caused by the white phase-noise component arising from both the optical amplifiers ASE noise and the thermal noise of the measurement system⁴⁴. The results indicate that a significant portion of the comb lines around -13 (equivalent 1565 nm wavelength) display a Lorentzian linewidth that is in fact smaller than that of the pump. Note that the location of the quiet mode is close to the simulation in Fig. 2d. The line located at -13 achieves the smallest phase noise, with a Lorentzian linewidth of ~1 kHz, corresponding to more than a threefold reduction of the pump’s value. The measurement is higher than the predictions (~0.4 kHz) provided in Fig. 2d. We believe the discrepancy is partly due to the TRN in the microresonator, which has a non-negligible contribution to the frequency range used for computing the Lorentzian linewidth⁴. Similar to the effect of the intensity noise, TRN leads to timing jitter or repetition rate change of soliton microcombs. Other effects that might contribute to the frequency noise dynamics include a frequency-dependent Q factor⁴⁵ or avoided mode crossings.

We continue with a quantitative analysis of the location of the fixed point by measuring the change of the soliton’s repetition rate with pump frequency, cf Eq. (5). Specifically, the repetition rate of the soliton is measured by electro-optic downconversion⁴⁶ as the pump is set at different values, which are measured with a wavelength meter. The results of this measurement are presented in Fig. 3c. The slope of the variation is positive, explaining why the fixed point appears on the red side of the pump, with the estimated fixed point $m_{\text{fix}} = -(d\nu_{\text{rep}}/d\nu_p)^{-1} = -15$. However, this measurement provides limited insight into the phase-to-phase transduction from the pump, because the temperature of the resonator is not the same when the detuning is changed. Such measurements are further addressed in the following

experiments. We modulated the pump laser with either a phase or intensity electro-optic modulator at an arbitrary specific single radio frequency before getting amplified by an EDFA. This introduces spikes in the $S_{\Delta\nu,m}(f)$ at the corresponding modulation frequency, at levels about 3 orders higher than the noise background. The measurement results are presented in Fig. 3d and e, corresponding to the phase and intensity modulation, respectively. The magnitude of the spike provides an indirect estimation of the influence of the pump's phase/amplitude noise on the Lorentzian linewidth of the corresponding comb line. One can see that while the intensity-to-phase noise transduction is symmetrically located around the pump, the phase-to-phase distribution attains its minimum at $m_{\text{fix}} = -18$, which is more in line with the simulations in Fig. 2a. Moreover, it is interesting to note that compared to the phase modulation spike, the intensity modulation spike fluctuates more. This can be explained as intensity-to-phase noise transduction is more sensitive to the detuning which may change slightly during the measurement.

Lorentzian linewidth and effective linewidth. The above analysis focused on the Lorentzian linewidth and ignored the low offset frequency noise contribution. In microresonators with small cavity volumes, the TRN has a significant contribution on the frequency noise PSD, specially at low frequencies^{27,47,48}. This noise source causes fluctuations in the location of the longitudinal modes and repetition rate of the soliton through the detuning parameter²¹. As a result, the PSD of the comb lines gets an additional contribution at low frequencies, see Fig. 4a (and Supplementary Fig. 4). To account for such non-white frequency noise, it is useful to calculate the effective linewidth of the comb lines $\Delta\nu_m^{\text{eff}}$ using the following definition⁴⁹:

$$\int_{\Delta\nu_m^{\text{eff}}}^{\infty} \frac{S_{\Delta\nu,m}(f)}{f^2} df = \frac{1}{\pi}. \quad (11)$$

The results are displayed in Fig. 4b (see also Supplementary Note 4), and compared to the results in Fig. 3b, reproduced again for convenience. Clearly, the non-white frequency noise region (or flicker noise) has a dominant contribution to the value of the effective linewidth. The distribution is symmetrical with respect to the pump. This is expected, and in line with previous reports²².

Frequency noise reduction in soliton microcombs. It is important to note that, the frequency noise reduction experienced by the comb lines nearby the fixed point takes place at all Fourier frequencies in the PSD. Not only is the Lorentzian linewidth reduced, but the low offset technical noise of the pump is also reduced according to Eq. (5). This is clearly demonstrated in Fig. 4a, where the pump displays a set of spikes in the PSD within the range 100 kHz–1 MHz. The spikes are significantly damped for the comb line -18, which is very close to the fixed point (see Supplementary Fig. 4c). This analysis points to the intriguing possibility of soliton microcombs to generate coherent oscillators on chip with a linewidth narrower than the pump itself—a feature that works more efficiently for broader linewidth lasers, cf Eq. (9). An experimental demonstration is given in Supplementary Fig. 3. When TRN contributes, such a reduction is however masked at low offset frequencies, see Fig. 4a, therefore, to fully capitalize on this characteristic, effective means to suppress TRN are needed, such as laser cooling^{21,50–52}, cavity dispersion engineering⁵³ or directly operating at cryogenic temperatures⁵⁴.

In the following, we investigate the laser cooling technique. The laser cooling is performed with an auxiliary laser coupled to the microresonator from the opposite direction, as schematically depicted in Fig. 5a. The cooling laser (Toptica, CTL 1550) has an on-chip power around 2 mW and is tuned into a resonance close to 1550 nm and kept blue detuned. The measured $S_{\Delta\nu,m}(f)$ for comb line $m = -18$ is shown in Fig. 5b. By applying the laser cooling technique, the frequency noise can be suppressed, but only up to a certain offset frequency. Take for example line $m = -18$, close to the fixed point. The laser cooling reduces up to an order of magnitude the frequency noise at low offset frequencies, but does not result in a further reduction in Lorentzian linewidth. This is more clearly observed when comparing the PSD of line $m = 6$, which is far away from the fixed point and, in the presence of laser cooling, its white frequency noise plateau is still above the corresponding level of the pump.

Discussion

In summary, we have analyzed the optical linewidth of soliton microcombs, including both the Lorentzian components and the low offset frequencies in the frequency noise spectral density. We

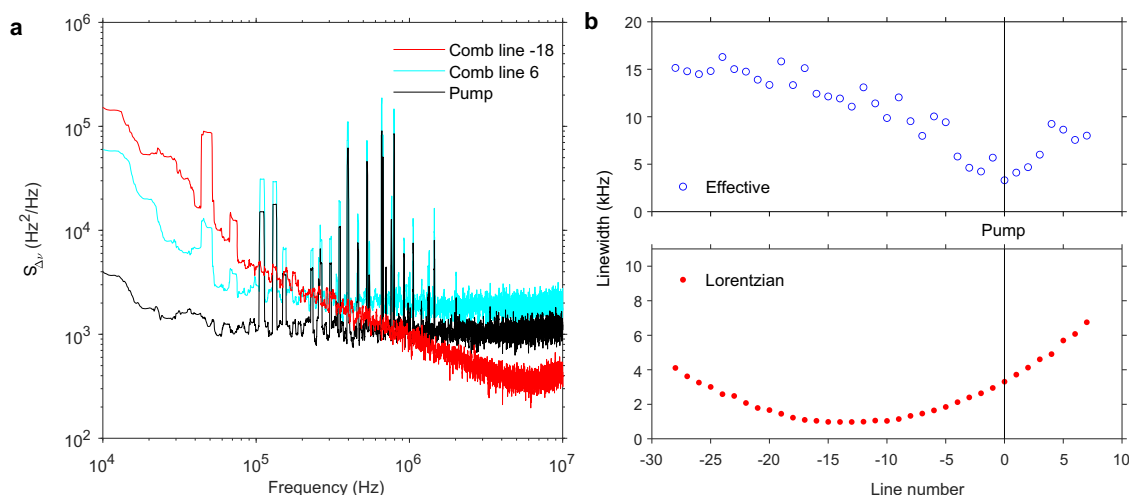


Fig. 4 Experimental comparison between effective and Lorentzian linewidth. **a** The frequency noise power spectral density $S_{\Delta\nu}^P(f)$ for two different comb lines. At low offset frequencies, all comb lines display higher frequency noise than the pump due to the TRN, while at high offset frequency range, some comb lines close to the quiet mode may have lower frequency noise than the pump. **b** Comparison between Lorentzian and effective linewidth. Because of the low-frequency noise, the effective linewidth is higher than the Lorentzian linewidth, and the linewidth distribution appears symmetrically located with respect to the pump.

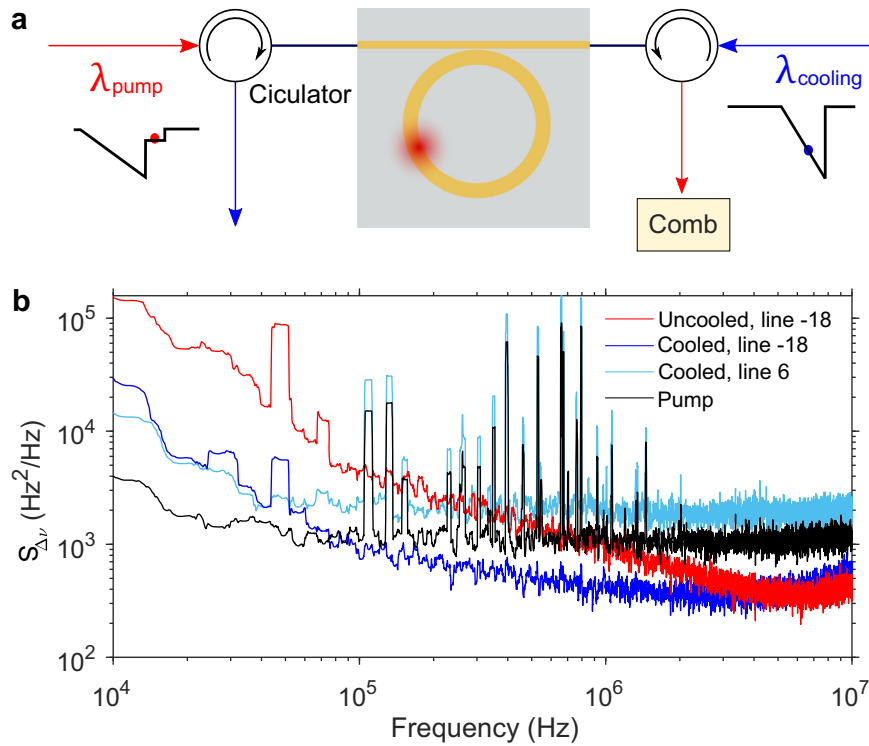


Fig. 5 Frequency noise reduction with laser cooling. **a** The schematic of the setup. An auxiliary laser (blue arrow) opposite to the pump (red arrow) is injected into the microresonator and blue-detuned to a cavity mode with the same family as the pump mode. $S_{\Delta\nu,-18}(f)$ without (red) and with (blue) laser cooling are shown in **b**. As reference, the pump frequency noise PSD $S_{\Delta\nu,6}^p(f)$ and $S_{\Delta\nu,6}(f)$ with laser cooling are shown as well.

discovered that the elastic-tape model, found previously for mode-locked lasers, does apply for soliton microcombs. This is not a mere translation of the model because in soliton microcombs the pump laser is coherently added to the soliton spectrum, which results in unexpected findings. In particular, because of the Raman self-frequency shift and dispersive-wave recoil, the model predicts the existence of a frequency region, potentially far away from the pump, where the soliton microcomb lines attain a Lorentzian linewidth below the one displayed by the pump laser.

This inherent property of soliton microcombs for optical phase noise reduction could be used to generate coherent oscillators derived from broad linewidth lasers. In practice, however, it is the TRN of the cavity that contributes the most at low-offset frequencies in the frequency noise power spectral density, resulting in a dominant contribution in the effective linewidth of the comb lines. This effect can be notwithstanding damped with the aid of a cooling laser. Further reduction of the TRN would be more helpful for this purpose, which might be realized by making the cavity with athermal material or increasing its size.

Methods

Resonator characteristics and operating condition. The SiN microring resonator is fabricated via subtractive processing as described in ref. 55. The radius of the microresonator used for the experiment is 100 μm , and the corresponding FSR is about 227.5 GHz. The height and the width of the SiN waveguide are 750 nm and 2100 nm, respectively, which result in a group velocity dispersion coefficient of $\beta_2 = -80 \text{ ps}^2/\text{km}$ for the TE_{00} mode. The average intrinsic Q-factor of the sample is 11.6 million and the total Q-factor is 8 million. Lensed fibers are used for coupling into and out of the on-chip SiN bus waveguide. The average coupling loss per facet is about 3.5 dB.

Theory and simulation. To apply the theoretical results corresponding to Eqs. (5)–(7) in Fig. 2a–d, the parameter m_{fix} was calculated using its definition, i.e., the derivative of repetition rate with respect to the pump’s frequency. The repetition rate was attained by monitoring the speed of the soliton, whose temporal position

t_p is calculated as⁵⁶

$$t_p = \frac{\int t|A(t)|^2 dt}{\int |A(t)|^2 dt} \tag{12}$$

The shot-noise-induced and RIN-induced timing jitter PSDs $S_{\text{tm}}^Q(f)$ and $S_{\text{tm}}^{\text{RIN}}(f)$ were obtained from simulations since there is no analytical result that includes the Raman self-frequency shift.

The simulation is performed with the Ikeda map³⁹. A full roundtrip evolution is divided into two steps including (1) the coupling between bus waveguide and resonator, (2) nonlinear propagation in the resonator over its circumference.

The coupling between bus waveguide and resonator can be described as⁴⁰

$$A_{m+1}(0, \tau) = \sqrt{\theta} A_m^{\text{in}} + \sqrt{1 - \theta} e^{i\phi_0} A_m(L, \tau), \tag{13}$$

where A_m stands for the amplitude (normalized to power) of intracavity field of m -th round trip, $\phi_0 = 2\pi(\nu_p - \nu_c)/\text{FSR}$, and $\theta = 2\pi\nu_p/(\text{FSR} \times Q_{\text{ex}})$ with Q_{ex} as the extrinsic quality factor. In each step, the pump phase noise can be included into A_m^{in} by setting $A_m^{\text{in}} = \sqrt{P_{\text{in}}} e^{i\phi_m}$. The white pump frequency noise can be simulated by generating a time-dependent pump phase through

$$\phi_{m+1} = \phi_m + \sqrt{2\pi\Delta\nu_p/\text{FSR}} \times \eta, \tag{14}$$

where η stands for a normally distributed random number.

The shot noise is treated via a semi-classical method described in refs. 56,57. Specifically, we add a noise field coupled to the resonator and set its random amplitude $\delta A^{\text{in}}(t)$ with statistics⁵⁶

$$\langle (\delta A^{\text{in}}(t))^* \delta A^{\text{in}}(t + \tau) \rangle = \frac{h\nu_p}{2} \delta(\tau). \tag{15}$$

Here h is the Planck constant. The coupling coefficient is set to $\sqrt{2\pi\nu_p(1/Q_{\text{ex}} + 1/Q_{\text{in}})/\text{FSR}}$, according to the fluctuation-dissipation theorem. This can be implemented in the split-step Fourier method with assignment of $\delta A^{\text{in}} = (\eta_1 + i\eta_2)\sqrt{h\nu_p \times N \times \text{FSR}/2}$ in the fast time domain, where $\eta_{1(2)}$ stands for a normally distributed random number and N is the number of discretization points.

To account for the frequency noise at the frequencies between 3 and 5 MHz contributed by the pump intensity noise, here we use the measured relative intensity noise (RIN) ($S_{\text{RIN}}^p = -127.5 \text{ dBc/Hz}$) in this region for the simulation. To incorporate the intensity noise into the simulation, a fluctuation term δP_{in} is added

to the input power P_{in} for each roundtrip satisfying

$$\delta P_m = P_{in} \sqrt{S_{RIN}^p \text{FSR}/2} \times \eta. \quad (16)$$

At each propagation step, the generalized nonlinear Schrödinger equation with (or without) inclusion of Raman scattering is solved^{31,58}:

$$\frac{\partial A}{\partial z} + \frac{\alpha}{2} A - i \sum_{n=1}^3 \frac{i^n \beta_n}{n!} \frac{\partial^n A}{\partial t^n} = i \gamma A(z, t) \times \int_0^\infty R(t') |A(z, t - t')|^2 dt'. \quad (17)$$

Here $R(t) = (1 - f_R)\delta(t) + f_R h_R(t)$, and $h_R(t) = (\tau_1^{-2} + \tau_2^{-2})\tau_1 \exp(-t/\tau_2) \sin(t/\tau_1)$, and the parameters have the same meaning as ref. ³¹. In the simulation, the parameters $\tau_1 = 15$ fs, $\tau_2 = 120$ fs, $f_R = 0.027$ are used as they match the measured optical spectrum. The remaining parameters are directly measured or simulated and have the following values: $P_{in} = 0.1$ W, $\gamma = 0.9\text{W}^{-1}\text{m}^{-1}$, $Q_{ex} = 3.15 \times 10^7$, $Q_{in} = 1.35 \times 10^7$, $\Delta\nu_p = 3.3$ kHz, $\nu_c - \nu_p = 626$ MHz.

To extract the phase noise information from the optical modes, around 8 million roundtrips were simulated in order to have reliable statistics at low offset frequencies. The phases of selected modes (nine modes equally spaced from comb line $m = -30$ to $m = 10$) were recorded every 512 roundtrips. With the recorded phases, we computed $S_{\Delta\nu,m}(f)$ and the Lorentzian linewidth for each comb line according to their definitions.

Frequency noise measurement and effective linewidth. With a coherent receiver, the complex amplitude of the beat between the laser and its delayed self is measured. Using the setup shown in Fig. 3a, the phase difference at two times of the laser under test can be directly extracted:

$$\Delta\phi(t) = \phi(t) - \phi(t - T), \quad (18)$$

where T stands for the time delay caused by a fiber loop with length of 27 km, as shown in Fig. 3a. An acousto-optic modulator driven at 27 MHz is used to shift the measured signal out of baseband.

According to Fourier analysis, we have

$$|\mathcal{F}\Delta\phi(t)|^2 = |\mathcal{F}\phi(t)|^2 \times 4\sin^2\left(\frac{2\pi fT}{2}\right). \quad (19)$$

Therefore, the $S_{\Delta\nu}(f)$ can be calculated by:

$$S_{\Delta\nu}(f) = \frac{f^2 |\mathcal{F}\Delta\phi(t)|^2}{4\sin^2(\pi fT)}. \quad (20)$$

In practice, to avoid the divergence point in Eq. (20), one could do an average for Eq. (19). Noting $\langle \sin^2(x) \rangle = 1/2$, we reach an approximated expression for $S_{\Delta\nu}(f)$:

$$S_{\Delta\nu}(f) = \frac{1}{2} \langle f^2 |\mathcal{F}\Delta\phi(t)|^2 \rangle_T, \quad (21)$$

where $\langle \cdot \rangle$ stands for the average over a period T .

The effective linewidth was obtained according to equation (10), by fitting the measured $S_{\Delta\nu,m}(f)$ with a function $a + b/(f + cf^2)$. To emphasize the generality of the definition of the effective linewidth, the spikes (as shown in Fig. 5) in the power spectral density were filtered out.

Data availability

The data necessary to reproduce the plots in this work can be accessed at <https://doi.org/10.5281/zenodo.6523268>.

Code availability

The code is available from the corresponding author upon reasonable request.

Received: 15 February 2021; Accepted: 16 May 2022;

Published online: 07 June 2022

References

- Schawlow, A. L. & Townes, C. H. Infrared and optical masers. *Phys. Rev.* **112**, 1940–1949 (1958).
- Zhang, Z. & Yariv, A. A general relation between frequency noise and lineshape of laser light. *IEEE J. Quantum Electron.* **56**, 1–5 (2020).
- Di Domenico, G., Schilt, S. & Thomann, P. Simple approach to the relation between laser frequency noise and laser line shape. *Appl. Opt.* **49**, 4801–4807 (2010).
- Jin, W. et al. Hertz-linewidth semiconductor lasers using CMOS-ready ultra-high-Q microresonators. *Nat. Photonics* **15**, 346–353 (2021).
- Gundavarapu, S. et al. Sub-hertz fundamental linewidth photonic integrated Brillouin laser. *Nat. Photonics* **13**, 60–67 (2019).
- Pfau, T., Hoffmann, S. & Noé, R. Hardware-efficient coherent digital receiver concept with feedforward carrier recovery for M-QAM constellations. *J. Light. Technol.* **27**, 989–999 (2009).
- Ludlow, A. D., Boyd, M. M., Ye, J., Peik, E. & Schmidt, P. O. Optical atomic clocks. *Rev. Mod. Phys.* **87**, 637 (2015).
- Diddams, S. A., Vahala, K. & Udem, T. Optical frequency combs: coherently uniting the electromagnetic spectrum. *Science* **369**, eaay3676 (2020).
- Fortier, T. & Baumann, E. 20 years of developments in optical frequency comb technology and applications. *Commun. Phys.* **2**, 153 (2019).
- Schmeissner, R., Roslund, J., Fabre, C. & Treps, N. Spectral noise correlations of an ultrafast frequency comb. *Phys. Rev. Lett.* **113**, 263906 (2014).
- Liehl, A. L. Deterministic nonlinear transformations of phase noise in quantum-limited frequency combs. *Phys. Rev. Lett.* **122**, 203902 (2019).
- Takushima, Y., Sotobayashi, H., Grein, M. E., Ippen, E. P. & Haus, H. A. Linewidth of mode combs of passively and actively mode-locked semiconductor laser diodes. In *Active and Passive Optical Components for WDM Communications IV*, vol. 5595, 213–227, <https://doi.org/10.1117/12.580046> (International Society for Optics and Photonics, 2004).
- Newbury, N. R. & Washburn, B. R. Theory of the frequency comb output from a femtosecond fiber laser. *IEEE J. Quantum Electron.* **41**, 1388–1402 (2005).
- Kim, J. & Song, Y. Ultralow-noise mode-locked fiber lasers and frequency combs: principles, status, and applications. *Adv. Opt. Photonics* **8**, 465–540 (2016).
- Del’Haye, P. et al. Optical frequency comb generation from a monolithic microresonator. *Nature* **450**, 1214–1217 (2007).
- Leo, F. et al. Temporal cavity solitons in one-dimensional Kerr media as bits in an all-optical buffer. *Nat. Photonics* **4**, 471–476 (2010).
- Herr, T. et al. Temporal solitons in optical microresonators. *Nat. Photonics* **8**, 145–152 (2014).
- Kippenberg, T. J., Gaeta, A. L., Lipson, M. & Gorodetsky, M. L. Dissipative Kerr solitons in optical microresonators. *Science* **361**, eaan8083 (2018).
- Del’Haye, P. et al. Octave spanning tunable frequency comb from a microresonator. *Phys. Rev. Lett.* **107**, 063901 (2011).
- Liao, P. et al. Dependence of a microresonator Kerr frequency comb on the pump linewidth. *Opt. Lett.* **42**, 779–782 (2017).
- Drake, T. E., Stone, J. R., Briles, T. C. & Papp, S. B. Thermal decoherence and laser cooling of Kerr microresonator solitons. *Nat. Photonics* **14**, 480–485 (2020).
- Nishimoto, K., Minoshima, K., Yasui, T. & Kuse, N. Investigation of the phase noise of a microresonator soliton comb. *Opt. Express* **28**, 19295–19303 (2020).
- Telle, H. R., Lipphardt, B. & Stenger, J. Kerr-lens, mode-locked lasers as transfer oscillators for optical frequency measurements. *Appl. Phys. B* **74**, 1–6 (2002).
- Karpov, M. et al. Raman self-frequency shift of dissipative Kerr solitons in an optical microresonator. *Phys. Rev. Lett.* **116**, 103902 (2016).
- Yi, X. et al. Single-mode dispersive waves and soliton microcomb dynamics. *Nat. Commun.* **8**, 14869 (2017).
- Matsko, A. B. & Maleki, L. On timing jitter of mode-locked Kerr frequency combs. *Opt. Express* **21**, 28862–28876 (2013).
- Huang, G. et al. Thermorefractive noise in silicon-nitride microresonators. *Phys. Rev. A* **99**, 061801 (2019).
- Brasch, V. et al. Photonic chip-based optical frequency comb using soliton Cherenkov radiation. *Science* **351**, 357–360 (2016).
- Matsko, A. B., Liang, W., Savchenkov, A. A., Eliyahu, D. & Maleki, L. Optical Cherenkov radiation in overmoded microresonators. *Opt. Lett.* **41**, 2907–2910 (2016).
- Yang, Q.-F., Yi, X., Yang, K. Y. & Vahala, K. Spatial-mode-interaction-induced dispersive waves and their active tuning in microresonators. *Optica* **3**, 1132–1135 (2016).
- Agrawal, G. P. *Nonlinear Fiber Optics*, 5th ed. (Academic, San Diego, 2012).
- Bao, C. et al. Soliton repetition rate in a silicon-nitride microresonator. *Opt. Lett.* **42**, 759–762 (2017).
- Kikuchi, K. Characterization of semiconductor-laser phase noise and estimation of bit-error rate performance with low-speed offline digital coherent receivers. *Opt. Express* **20**, 5291–5302 (2012).
- Corwin, K. L. et al. Fundamental noise limitations to supercontinuum generation in microstructure fiber. *Phys. Rev. Lett.* **90**, 113904 (2003).
- Dudley, J. M., Genty, G. & Coen, S. Supercontinuum generation in photonic crystal fiber. *Rev. Mod. Phys.* **78**, 1135 (2006).
- Bao, C. et al. Quantum diffusion of microcavity solitons. *Nat. Phys.* **17**, 462–466 (2021).
- Jeong, D. et al. Ultralow jitter silica microcomb. *Optica* **7**, 1108–1111 (2020).
- Jia, K. et al. Photonic flywheel in a monolithic fiber resonator. *Phys. Rev. Lett.* **125**, 143902 (2020).
- Ikeda, K. Multiple-valued stationary state and its instability of the transmitted light by a ring cavity system. *Opt. Commun.* **30**, 257–261 (1979).
- Hansson, T. & Wabnitz, S. Dynamics of microresonator frequency comb generation: models and stability. *Nanophotonics* **5**, 231–243 (2016).

41. Lundberg, L. et al. Phase-coherent lightwave communications with frequency combs. *Nat. Commun.* **11**, 201 (2020).
42. Brajato, G., Lundberg, L., Torres-Company, V., Karlsson, M. & Zibar, D. Bayesian filtering framework for noise characterization of frequency combs. *Opt. Express* **28**, 13949–13964 (2020).
43. Joshi, C. et al. Thermally controlled comb generation and soliton modelocking in microresonators. *Opt. Lett.* **41**, 2565–2568 (2016).
44. Newbury, N. R. & Swann, W. C. Low-noise fiber-laser frequency combs (invited). *J. Opt. Soc. Am. B* **24**, 1756–1770 (2007).
45. Matsko, A. B. & Maleki, L. Noise conversion in Kerr comb RF photonic oscillators. *J. Opt. Soc. Am. B* **32**, 232–240 (2015).
46. Del’Haye, P., Papp, S. B. & Diddams, S. A. Hybrid electro-optically modulated microcombs. *Phys. Rev. Lett.* **109**, 263901 (2012).
47. Gorodetsky, M. L. & Grudinin, I. S. Fundamental thermal fluctuations in microspheres. *J. Opt. Soc. Am. B* **21**, 697–705 (2004).
48. Matsko, A. B., Savchenkov, A. A., Yu, N. & Maleki, L. Whispering-gallery-mode resonators as frequency references. i. fundamental limitations. *J. Opt. Soc. Am. B* **24**, 1324–1335 (2007).
49. Hjelme, D. R., Mickelson, A. R. & Beausoleil, R. G. Semiconductor laser stabilization by external optical feedback. *IEEE J Quantum Electron.* **27**, 352–372 (1991).
50. Sun, X., Luo, R., Zhang, X.-C. & Lin, Q. Squeezing the fundamental temperature fluctuations of a high-Q microresonator. *Phys. Rev. A* **95**, 023822 (2017).
51. Lei, F., Ye, Z. & Torres-Company, V. Thermal noise reduction in soliton microcombs via laser self-cooling. *Opt. Lett.* **47**, 513–516 (2022).
52. Nishimoto, K., Minooshima, K., Yasui, T. & Kuse, N. Thermal control of a Kerr microresonator soliton comb via an optical sideband. *Opt. Lett.* **47**, 281–284 (2022).
53. Stone, J. R. & Papp, S. B. Harnessing dispersion in soliton microcombs to mitigate thermal noise. *Phys. Rev. Lett.* **125**, 153901 (2020).
54. Moille, G. et al. Kerr-microresonator soliton frequency combs at cryogenic temperatures. *Phys. Rev. Appl.* **12**, 034057 (2019).
55. Ye, Z., Twayana, K., Andrekson, P. A. & Torres-Company, V. High-Q Si₃N₄ microresonators based on a subtractive processing for Kerr nonlinear optics. *Opt. Express* **27**, 35719–35727 (2019).
56. Paschotta, R. Noise of mode-locked lasers (part I): numerical model. *Appl. Phys. B* **79**, 153–162 (2004).
57. Drummond, P. & Corney, J. F. Quantum noise in optical fibers. I. stochastic equations. *J. Opt. Soc. Am. B* **18**, 139–152 (2001).
58. Dudley, J. M. & Taylor, J. R. *Supercontinuum Generation in Optical Fibers* (Cambridge University Press, 2010).

Acknowledgements

The devices demonstrated in this work were fabricated at Myfab Chalmers. We acknowledge funding support from the European Research Council (ERC, CoG GA 771410), Knut Alice Wallenbergs Foundation (59201011), and the Swedish Research Council (2015-00535, 2016-06077, 2020-00453).

Author contributions

F.L. conducted the experiment with input from Z.Y., Ó.B.H.; F.L. provided the theoretical model and numerical simulations with input from Ó.B.H.; Z.Y. and M.G. designed and fabricated the SiN devices; A.F. developed the phase noise measurement system. All authors discussed the results. F.L. and V.T.-C. prepared the manuscript with input from all co-authors. V.T.-C. supervised this project.

Funding

Open access funding provided by Chalmers University of Technology.

Competing interests

The authors declare no competing interests.

Additional information

Supplementary information The online version contains supplementary material available at <https://doi.org/10.1038/s41467-022-30726-5>.

Correspondence and requests for materials should be addressed to Victor Torres-Company.

Peer review information *Nature Communications* thanks Jungwon Kim and the other anonymous 3 reviewer(s) for their contribution to the peer review of this work.

Reprints and permission information is available at <http://www.nature.com/reprints>

Publisher’s note Springer Nature remains neutral with regard to jurisdictional claims in published maps and institutional affiliations.



Open Access This article is licensed under a Creative Commons Attribution 4.0 International License, which permits use, sharing, adaptation, distribution and reproduction in any medium or format, as long as you give appropriate credit to the original author(s) and the source, provide a link to the Creative Commons license, and indicate if changes were made. The images or other third party material in this article are included in the article’s Creative Commons license, unless indicated otherwise in a credit line to the material. If material is not included in the article’s Creative Commons license and your intended use is not permitted by statutory regulation or exceeds the permitted use, you will need to obtain permission directly from the copyright holder. To view a copy of this license, visit <http://creativecommons.org/licenses/by/4.0/>.

© The Author(s) 2022